Journal of the Korean Physical Society, Vol. 67, No. 5, September 2015, pp. 843∼853

Development of a Free-boundary Tokamak Equilibrium Solver for Advanced Study of Tokamak Equilibria

Young Mu Jeon*
National Fusion Research Institute, Daejeon 305-333, Korea

(Received 11 March 2015, in final form 8 July 2015)

A free-boundary Tokamak equilibrium solver (TES), developed for advanced study of tokamak equilibra, is described with two distinctive features. One is a generalized method to resolve the intrinsic axisymmetric instability, which is encountered in all equilibrium calculations with a free-boundary condition. The other is an extension to deal with a new divertor geometry such as snow-flake or X divertors. For validations, the uniqueness of a solution is confirmed by the independence of variations in the computational domain, the mathematical correctness and accuracy of equilibrium profiles are checked by using a direct comparison with an analytic equilibrium known as a generalized Solov'ev equilibrium, and the governing force balance relation is tested by examining the intrinsic axisymmetric instabilities. As an application of an advanced equilibrium study, a snow-flake divertor configuration that requires a second-order zero of the poloidal magnetic flux is discussed in the circumstance of the Korea superconducting tokamak advanced research (KSTAR) coil system.

PACS numbers: 52.55.Fa, 52.55.-s, 52.40.Hf
Keywords: Tokamak equilibrium, Free-boundary equilibrium, TES, Solov'ev equilibrium, Snow-flake divertor
DOI: 10.3938/jkps.67.843

I. INTRODUCTION

In tokamak physics, plasma equilibrium is a fundamental and essential element to understand not only the basic equilibrium properties but also various plasma phenomena such as magnetohydrodynamic (MHD) instabilities, plasma transport and turbulence, plasma flows and waves, and so on. Therefore, various numerical or analytical equilibrium studies [1] have been conducted for a long time since the axisymmetric plasma equilibrium relation was established in a general form, known as the Grad-Shafranov equation [2,3].

Depending on the characteristics of applications, we can categorize the studies into two types of problems. One, so-called 'fixed boundary equilibrium', is solving an equilibrium by assuming that the plasma boundary or plasma region is known. Thus, the external equilibrium field is ignored, and the internal equilibrium profiles and flux distributions are the main concerns. The other, so-called 'free boundary equilibrium', is solving the equilibrium with a unknown plasma boundary. Hence, the plasma's position and shape (*i.e.*, the plasma region) are obtained as a solution in addition to the equilibrium profiles and the flux distributions.

Due to the importance of equilibrium as a basis for various physics studies, the majority of equilibrium studies have been devoted to fixed-boundary equilibrium problems, while the free-boundary equilibrium solutions were of less interest. However, recently, the free-boundary equilibrium analysis has been resurrected because of new demands. For instance, another type of equilibrium with new topological features, the so-called snow-flake (SF) divertor [4] or X-divertor [5] equilibrium, has recently been proposed and actively studied in various devices [6, 7]. Especially, because the SF divertor configuration requires a second-order zero of the poloidal magnetic field, it is now an important issue that should be addressed in terms of a free-boundary tokamak equilibrium [8]. Accordingly, a free-boundary Tokamak Equilibrium Solver, called TES, has been developed with an emphasis on applications to a design work for plasma equilibrium control and for advanced equilibrium study. This code features two distinctive functionalities: a generalized method for stabilization of axisymmetric instabilities, and an extension to deal with a second-order zero of the poloidal magnetic field. Note that all analyses and interpretations in this paper are based on the Korea superconducting tokamak advanced research (KSTAR) tokamak [9].

In Section II, the numerical solution methods and procedures used in TES are described for two types of free-boundary equilibrium problems, *i.e.*, *ideally free* and *semi-free* boundary problems that will be defined therein. Most of the numerical techniques and issues are well known, so only a brief description of each issues will be given. For validations of the TES code, a direct com-

*E-mail: ymjeon@nfri.re.kr; Fax: +82-42-879-5127

parison with a generalized analytic solution, in addition to the uniqueness of a solution, is described in Sec. III. In Sec. IV, an intrinsic axisymmetric instability encountered during the numerical procedure is tested by examining the variations of the plasma equilibria, and a generalized stabilization method is introduced and tested. In Sec. V, an extended feature to deal with a snow-flake divertor is explained and discussed, followed by a summary and conclusion in Sec. VI.

II. A SOLUTION METHOD IN TES

A basic numerical method and procedure has been well established for an axisymmetric tokamak plasma equilibrium with a free boundary condition [10–12]. The mathematical and the numerical treatments used in TES code are also basically in line with those in the references, except for some improved and extended features. Therefore, in this section, the basic numerical treatments and procedures used in the TES code are described briefly.

1. Force Balance Relation for the Free-boundary Plasma Equilibrium

In a toroidally axisymmetric system like a tokamak, the force balance relation of a plasma, *i.e.*, plasma equilibrium, can be expressed by a second-order partial differential equation, known as the Grad-Shafranov equation [2, 3], by using a cylindrical coordinate system (R, ϕ, Z) with an ignorable (due to axisymmetry) toroidal angle coordinate ϕ:

$$\triangle^* \psi(R,Z) = -\mu_0 R J_{\phi,pl}(R,Z), \quad (1)$$

$$J_{\phi,pl}(R,Z) = Rp'(\psi) + \frac{F(\psi)F(\psi)'}{\mu_0 R}, \quad (2)$$

where the poloidal flux function (equal to the poloidal magnetic flux divided by 2π) is defined by $\psi(R,Z) \equiv RA_\phi(R,Z)$ from $B = \nabla \times A$ (*i.e.*, $\nabla \cdot B = 0$), the Shafranov operator is defined by $\triangle^* \equiv R^2 \nabla \cdot \frac{\nabla}{R^2}$, and the prime denotes $g' \equiv \frac{\partial g}{\partial \psi}$. In addition, $p(\psi)$ is the isotropic plasma pressure, $F(\psi) \equiv RB_\phi$ is a toroidal field function, and $J_{\phi,pl}(R,Z)$ is the toroidal current density of the plasma. The fact that the $J_{\phi,pl}(R,Z)$ as a source term in Eq. (1) has a strong dependency on $\psi(R,Z)$ by Eq. (2) gives rise to a strong non-linearity of the equations.

In order to deal with a free boundary condition in an equilibrium calculation, we generalize Eq. (1) by including arbitrary toroidal conductor currents as follows:

$$\begin{aligned} \triangle^* \psi(R,Z) &= -\mu_0 R J_\phi(R,Z), \\ J_\phi(R,Z) &= J_{\phi,pl}(R,Z) + J_{\phi,cond}(R,Z), \end{aligned} \quad (3)$$

where $J_{\phi,cond}(R,Z)$ is the toroidal current density for a conductor. The toroidal conductor can be any toroidal current source that may affect the equilibrium force balance, such as poloidal field (PF) coil currents or axisymmetric eddy currents on surrounding conductor structures. Assuming discrete conductors with uniform current distributions inside, we can express the toroidal conductor current density as

$$J_{\phi,cond}(R,Z) = \sum_{k=1}^{N_{cond}} J_{cond,k}(R,Z), \quad (4)$$

$$J_{cond,k}(R,Z) = \begin{cases} I_{cond,k}/S_k & \text{if } (R,Z) \in \Omega_{cond,k} \\ 0 & \text{otherwise}, \end{cases}$$

where $J_{cond,k}$, $I_{cond,k}$, S_k, and $\Omega_{cond,k}$ are the toroidal current density, the toroidal current, the cross-sectional area, and the domain region of the k-th conductor, respectively.

Meanwhile, the toroidal current density of the plasma, $J_{\phi,pl}$ in Eq. (2), can be put into a canonical form [13] as shown below:

$$J_{\phi,pl}(R,Z) = \begin{cases} \lambda \left[\beta_0 \frac{R}{R_{geo}} \tilde{j}_{\mathrm{P}}(\psi,\psi_a,\psi_b) + (1-\beta_0) \frac{R_{geo}}{R} \tilde{j}_{\mathrm{F}}(\psi,\psi_a,\psi_b) \right] & \text{if } (R,Z) \in \Omega_{pl} \\ 0 & \text{otherwise}, \end{cases} \quad (5)$$

with $\tilde{j}_{\mathrm{P}}(\psi,\psi_a,\psi_b) \equiv (1-\psi_s^{\alpha_m})^{\alpha_n}$ and $\tilde{j}_{\mathrm{F}}(\psi,\psi_a,\psi_b) \equiv \left(1-\psi_s^{\beta_m}\right)^{\beta_n}$, where R_{geo} is the major radius as a reference length scale, ψ_a the flux per radian at the plasma magnetic axis, and ψ_b the flux per radian at the plasma boundary. The λ and the β_0 are adjustable variables to satisfy the equilibrium constraints which will be discussed later, while the $\alpha_m, \alpha_n, \beta_m$, and β_n are input variables specified by the user. Note that $J_{\phi,pl}(R,Z)$ is automatically set to zero at the plasma's boundary in this form by using a normalized poloidal flux, $\psi_s \equiv (\psi - \psi_a)/(\psi_b - \psi_a)$.

In short, a free-boundary plasma equilibrium can be

obtained by solving Eq. (3) with a toroidal current density specified by Eqs. (4) and (5). The corresponding equilibrium profiles, such as $p(\psi)$ and $F(\psi)$, can be obtained from Eqs. (2) and (5).

2. Numerical Approximation by Discretization

The governing equation described above, *i.e.*, Eq. (3), can be thought of as a 2D Poisson's equation in toroidal geometry. Thus it can be easily solved by using various numerical methods if the source term is known. For numerical treatments, the equation is converted to a linear algebraic equation by using the centered finite difference method (FDM) [14] on a rectangular computational domain in (R, Z) space, where the grids, (R_l, Z_j), are built by

$$\begin{aligned} &R_l = R_{min} + \Delta R \times (l-1), \\ &\Delta R \equiv (R_{max} - R_{min})/(N_R - 1), \\ &Z_j = Z_{min} + \Delta Z \times (j-1), \\ &\Delta Z \equiv (Z_{max} - Z_{min})/(N_Z - 1), \end{aligned} \tag{6}$$

with $l = 1, \cdots, N_R$ and $j = 1, \cdots, N_Z$. Then, the algebraic equation obtained by using the FDM can be expressed as

$$\begin{aligned} \frac{1}{(\Delta Z)^2}\psi_{j-1,l} &+ \left(\frac{1}{(\Delta R)^2} + \frac{1}{2R_l(\Delta R)}\right)\psi_{j,l-1} - \left\{2\left(\frac{1}{(\Delta R)^2} + \frac{1}{(\Delta Z)^2}\right)\right\}\psi_{j,l} \\ &+ \left(\frac{1}{(\Delta R)^2} - \frac{1}{2R_l(\Delta R)}\right)\psi_{j,l+1} + \frac{1}{(\Delta Z)^2}\psi_{j+1,l} = -\mu_0 R_l J_{\phi j,l} \ , \end{aligned} \tag{7}$$

where $\psi_{j,l} = \psi(R_l, Z_j)$ and $J_{\phi j,l} = J_\phi(R_l, Z_j)$ with $l = 2, \cdots, N_R - 1$ and $j = 2, \cdots, N_Z - 1$. This algebraic equation can be solved by either using a matrix inversion after reforming it in the form of $\mathbf{Ax} = \mathbf{b}$ or using an iterative method such as a multi-grid method [14] or a double cyclic reduction [15], with an appropriate boundary condition. In the TES code, the successive-over-relaxation (SOR) method [14] is used as a basic numerical scheme for simplicity.

3. Iterative Solution for Non-linearity

To solve Eq. (7) in the given form, one must know the source term on the right hand side. However, the plasma part of the source term has a strong nonlinear dependency on $\psi_{j,l}$ according to Eq. (2) or (5). To deal with this non-linearity, we adopted an iteractive method known as Picard iteration [16]. Then, Eq. (7) is expressed as

$$\begin{aligned} \frac{1}{(\Delta Z)^2}\psi^{(n)}_{j-1,l} &+ \left(\frac{1}{(\Delta R)^2} + \frac{1}{2R_l(\Delta R)}\right)\psi^{(n)}_{j,l-1} - \left\{2\left(\frac{1}{(\Delta R)^2} + \frac{1}{(\Delta Z)^2}\right)\right\}\psi^{(n)}_{j,l} \\ &+ \left(\frac{1}{(\Delta R)^2} - \frac{1}{2R_l(\Delta R)}\right)\psi^{(n)}_{j,l+1} + \frac{1}{(\Delta Z)^2}\psi^{(n)}_{j+1,l} \\ &= -\mu_0 R_l J^{(n)}_{\phi j,l}\left(\psi^{(n-1)}_{j,l}\right), \end{aligned} \tag{8}$$

where (n) indicates the n-th Picard iteration. Note that the source term in the n-th iteration, $J^{(n)}_{\phi j,l}$, is expressed as a function of $\psi^{(n-1)}_{j,l}$, *i.e.*, the poloidal flux in the (n-1)th iteration. Hence, the $\psi^{(n)}$ is obtained from Eq. (8) using $J^{(n)}_\phi$ that was evaluated from $\psi^{(n-1)}$. Then, the $J^{(n+1)}_\phi$ is updated by using the refreshed $\psi^{(n)}$ and is applied back to Eq. (8) as an updated source term. This recursive iteration is continued until a convergence criterion, $\left\|\psi^{(n)} - \psi^{(n-1)}\right\| < \epsilon$, is satisfied.

4. Boundary Conditions

In general, the boundary condition in a free-boundary equilibrium calculation is not constant and varies due to changes in the plasma's boundary and its equilibrium profiles during the numerical iterations while in a fixed

boundary equilibrium, it is usually fixed to zero ($\psi_{bc} = 0$). The Dirichlet boundary condition on the edge of a computational domain can be provided directly by using a Green's function formulation [17]:

$$\psi(R,Z) = \iint G(R,Z;R',Z')J_\phi(R',Z')dR'dZ', \quad (9)$$

where $G(R,Z;R',Z')$ is the free-space Green's function, which gives the poloidal flux at (R,Z) from a unit toroidal current source at (R',Z'). The free-space Green's function is defined by

$$\begin{aligned} G(R,Z;R',Z') &= \frac{\mu_0}{2\pi}\frac{\sqrt{RR'}}{k}\left[\left(2-k^2\right)K(k) - 2E(k)\right], \\ k^2 &\equiv \frac{4RR'}{\left(R+R'\right)^2 + \left(Z-Z'\right)^2}, \end{aligned} \quad (10)$$

where $K(k)$ and $E(k)$ are elliptic integrals of the first and the second kind [14], respectively. With this, the poloidal flux at the boundary of the computational domain can be directly obtained by taking into account both the plasma and the conductor currents as follows:

$$\begin{aligned} &\psi^{(n)}_{bndry}(R_b,Z_b) \\ &= \int_{\Omega'_{pl}} G(R_b,Z_b;R',Z')J^{(n)}_{\phi,pl}(R',Z')d\Omega'_{pl} \\ &+ \int_{\Omega'_{cond}} G(R_b,Z_b;R',Z')J^{(n)}_{\phi,cond}(R',Z')d\Omega'_{cond}, \end{aligned} \quad (11)$$

where (R_b,Z_b) is the boundary point of the computational domain. Note that $J^{(n)}_{\phi,pl}(R',Z')$ is different in every steps of Picard iterations while $J^{(n)}_{\phi,cond}(R',Z')$ does not change unless the plasma boundary is specified, which will be discussed later.

5. Determination of the Plasma Boundary

For a stable convergence of the solution, accurately determining the plasma region or boundary in terms of ψ_b in every steps of Picard iteration is important. Generally, a plasma boundary is formed either by limiters (a limited plasma) or by magnetic fields with an X-point (a diverted plasma). If $I_p > 0$, the poloidal flux, $\psi(R,Z)$, has a convex distribution inside the plasma; thus, $\psi_a > \psi_b$. Therefore, the ψ_b is defined by the maximum value among all poloidal fluxes from limiters and from X-points. When $I_p < 0$, the ψ_b is defined by the minimum value according to the same logic.

More precisely, both the magnetic axis and the X-point have a null-field ($|\nabla\psi|^2 = 0$) while they have different signs of the second-derivatives [10] defined by

$$S(R,Z) \equiv \left(\frac{\partial^2\psi}{\partial R^2}\right)\left(\frac{\partial^2\psi}{\partial Z^2}\right) - \left(\frac{\partial^2\psi}{\partial R\partial Z}\right)^2. \quad (12)$$

If $S > 0$, the field-null point is a magnetic axis (ψ_a). Otherwise ($S < 0$), it is an X-point. The accurate location of the magnetic axis or the X-point is determined by using Powell's conjugate direction method [14] based on a 2D bicubic interpolation.

6. Constraints on the Plasma Equilibrium

For a unique equilibrium solution for Eq. (2), a few constraints on plasma equilibrium quantaties are necessary. Considering the functional form of Eq. (5), we apply two constraints, the total plasma current and the poloidal plasma beta constraints. Note that the equilibrium constraints could be different when a different functional form of $J_{\phi,pl}(R,Z)$ is used instead of Eq. (5). For instance, if the $q(\psi)$ profile is used in $J_{\phi,pl}(R,Z)$, then $q_a = q(\psi_a)$ could be used as another appropriate constraint [18].

The constraints can be expressed as

$$I_p = \int_{\Omega_{pl}} J_{\phi,pl}(\lambda,\beta_0)d\Omega, \quad (13a)$$

$$\beta_p = \frac{\langle p(\beta_0)\rangle}{\langle B_p^2\rangle_{\psi_a}/2\mu_0}, \quad (13b)$$

where $\mu_0 = 4\pi\times10^{-7}[N/A^2]$ is the permeability of vacuum, a the minor radius, and B_p the poloidal magnetic field. The bracket $\langle\cdot\rangle$ means an average over a magnetic surface. Therefore, if these two equations are combined, the β_0 and the λ can be determined, thus giving a unique solution.

7. External Equilibrium Fields with a Specified Plasma Boundary

In principle, for a free-boundary equilibrium problem, the plasma boundary is found as a part of the solutions under given external equilibrium fields. In practice, however, solving the equilibrium with a specified plasma boundary is more useful and convenient. In this study, we distinguish them by calling the former an *ideally-free* boundary problem while calling the latter a *semi-free* boundary problem. In the case of a *semi-free* boundary, the external coil currents are adjusted to provide the required equilibrium field. If a plasma boundary is specified in a series of points, the required external equilibrium field currents can be determined by solving the minimization problem shown below:

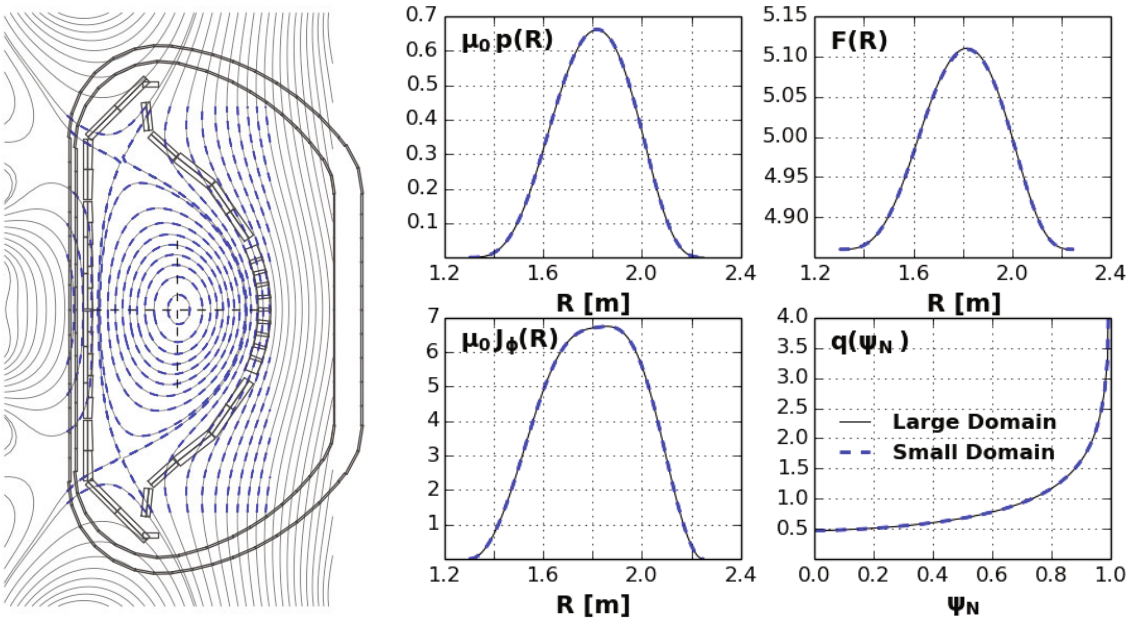

Fig. 1. (Color online) Two free-boundary equilibria obtained by using TES with identical equilibrium constraints are directly compared. On the left, the poloidal magnetic flux in a large computational domain (black solid line) is compared with that in a small computational domain (blue dotted line). On the right, several equilibrium profiles are directly compared, such as the isotropic pressure, the toroidal field function, the toroidal current density, and the safety factor profile.

$$\min_{\Delta I_{\rm coil}} \Bigg[\sum_{j=1}^{N_{\rm bndry}} \left\{ \sum_{i=1}^{N_{\rm coil}} \Big(G(R_j,Z_j;R_i,Z_i)\cdot \Delta I_{{\rm coil},i} \Big) - \Delta\psi(R_j,Z_j) \right\}^2 + \sum_{j=1}^{N_{\rm Xpt}} \left\{ \sum_{i=1}^{N_{\rm coil}} \Big(G_{B_R}(R_j,Z_j;R_i,Z_i)\cdot \Delta I_{{\rm coil},i} \Big) - B_R(R_j,Z_j) \right\}^2 + \sum_{j=1}^{N_{\rm Xpt}} \left\{ \sum_{i=1}^{N_{\rm coil}} \Big(G_{B_Z}(R_j,Z_j;R_i,Z_i)\cdot \Delta I_{{\rm coil},i} \Big) - B_Z(R_j,Z_j) \right\}^2 + \gamma^2 \textstyle\sum_{i=1}^{N_{\rm coil}} \Big(\Delta I_{{\rm coil},i} \Big)^2 \Bigg], \tag{14}$$

where (R_j, Z_j) is the specified j-th boundary point, $\Delta\psi(R_j,Z_j) = \psi_b - \psi(R_j,Z_j)$ is the poloidal flux error on the point, $B_R(R_j,Z_j)$ and $B_Z(R_j,Z_j)$ are the radial and the vertical magnetic fields there, respectively, and γ is a Tikhonov parameter for regularization [19]. If an X-point is specified as a part of the plasma boundary, then the radial and the vertical magnetic fields at the point should be zeros. This constraint is added as the second and the third terms in Eq. (14) with $G_{B_R} \equiv -\frac{1}{R}\frac{\partial G}{\partial Z}$ and $G_{B_Z} \equiv +\frac{1}{R}\frac{\partial G}{\partial R}$. From this, the external equilibrium field currents are obtained as $I^{(n)}_{{\rm coil},j} = I^{(n-1)}_{{\rm coil},j} + \Delta I_{{\rm coil},j}$, where $I^{(n-1)}_{{\rm coil},j}$ is the coil currents in the $(n-1)$th Picard iteration.

III. VALIDATIONS OF TES

A free-boundary TES has been developed based on the numerical methods and procedures described above. For the validations of this code, the uniqueness of a solution is firstly checked by examining the independence of the variations of computation domains, and the mathematical correctness and accuracy of equilibrium profiles are assessed by using a direct comparison with an analytic equilibrium solution.

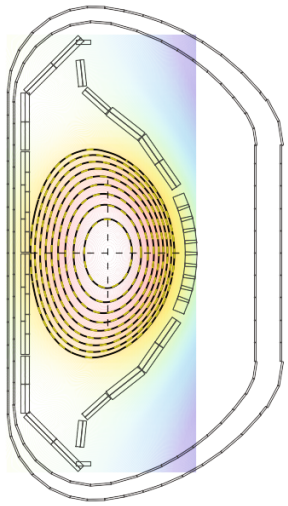

Fig. 2. (Color online) The poloidal magnetic flux obtained from TES (black solid line) is compared directly with the analytic flux from Solovev's equilibirum (yellow dotted line). The filled contour plot with a rectangular boundary shows the full distribution of poloidal magnetic flux, including a vacuum region, which are obtained from TES.

1. Uniqueness of a Solution under Numerical Variations

Because we are solving the problem in a numerical approach, one fundamental test, which is seldom seen in the related literature, is to examine if it provides an identical result, independent of the number of grids or the change of the computational domain. This is particularly essential and critical when a free boundary condition is imposed.

A comparison of the two free-boundary equilibrium solutions, one in a large and the other in a small computational domain, is shown in Fig. 1 where $I_p = -2.0$ MA, $B_T = -2.7$ T, $a = 0.48$ m, and $\beta_p = 0.5$ with a large elongation $\kappa = 2.0$. The poloidal magnetic fluxes are compared on the left, and several equilibrium profiles are compared on the right. The solution for a large computational domain (black solid line) was obtained in $0.7 \le R \le 2.8$ m, $-1.9 \le Z \le +1.9$ m with $N_R \times N_Z = 65 \times 85$ while the one for a small computational domain (cyan dotted line) in $1.1 \le R \le 2.4$ m, $-1.3 \le Z \le +1.3$ m with $N_R \times N_Z = 45 \times 65$. As expected, the poloidal magnetic fluxes and the equilibrium profiles are shown to be almost identical for both. Therefore, the equilibrium obtained by using TES is confirmed to provide a unique solution, independently of any change in the computational domain or the grid size.

2. Benchmark with an Analytic Solution

For a direct validation of TES, an analytic fixed boundary equilibrium solution, known as a generalized Solov'ev equilibrium [20], is considered and compared with a TES result. Note that this checks the mathematical correctness and accuracy of the solution from TES. The pressure and the toroidal field function in the analytic solution are assumed to be constant:

$$-\mu_0 \frac{\partial p}{\partial \psi} = A_1, \quad F\frac{\partial F}{\partial \psi} = A_2. \tag{15}$$

Then, the equilibrium solution can be expressed explicitly as follows:

$$\begin{aligned}\psi(R,Z) &= c_1 + c_2 R^2 + c_3(R^4 - 4R^2Z^2) \\ &+ c_4\left[R^2\ln(R) - Z^2\right] + \frac{R^4}{8}A_1 - \frac{Z^2}{2}A_2,\end{aligned} \tag{16}$$

where four constants, c_i, $i = 1, \cdots, 4$ are determined to satisfy the boundary conditions from specified plasma boundary, and two other parameters, A_1 and A_2, are adjusted to meet the equilibrium constraints. The four boundary conditions, with a modification for the comparison, are given by $\psi(R_{in}, Z_{in}) = \psi(R_{out}, Z_{out}) = \psi(R_{top}, Z_{top}) = \psi_b$ and $\frac{\partial\psi}{\partial R}\big|_{(R_{top},Z_{top})} = 0$, where *in*, *out*, and *top* are the inner-, the outer-, and the topmost boundary points, respectively. The equilibrium constraints are the total plasma currents I_p and the poloidal beta β_p:

$$I_p = \int_{\Omega_{pl}} J_\phi dRdZ = -\left(\int_{\Omega_{pl}} \left(\frac{R}{\mu_0}\right) dRdZ\right) A_1 + \left(\int_{\Omega_{pl}} \left(\frac{1}{\mu_0 R}\right) dRdZ\right) A_2, \tag{17a}$$

$$\beta_p = \frac{8\pi}{\mu_0}\frac{\int p\, dRdZ}{I_p^2} = \left(\frac{8\pi}{(\mu_0 I_p)^2}\int(\psi_b - \psi)dRdZ\right) A_1, \tag{17b}$$

with appropriate values of A_1 and A_2.

The poloidal magnetic fluxes obtained from TES and the analytic solution are directly compared in Fig. 2,

where $I_p = 0.5$ MA, $B_T = 2.7$ T, and $\beta_p = 0.5$, with elongation $\kappa = 1.45$ and minor radius $a = 0.5$ m in a limited configuration (*i.e.*, without a null point). The full distribution (including the vacuum region) of the poloidal magnetic flux from TES is shown as a filled contour plot with a rectangular boundary to show that it is, indeed, a free-boundary solution. The poloidal magnetic fluxes in the plasma region are directly compared by overlapping them; one is from TES (black solid line) and the other from the analytic solution (yellow dotted line). As shown, the two results are indistinguishable; thus, the difference is negligible. This confirms that the equilibrium information inside the plasma region, as obtained by using TES, is consistent with those from analytic calculations.

In summary, for validations, firstly we have shown that an identical solution is obtained independent of the number of computational grids and the size of the computational domain. Secondly, the comparison with the analytic equilibrium solution confirms that the solution is highly accurate and consistent with that obtained from a theoretical analysis.

IV. AXISYMMETRIC INSTABILITY AND ITS STABILIZATION

1. Axisymmetric Instability of a Shaped Plasma Equilibrium

A tokamak plasma equilibrium has 2D axisymmetric, instrinsic instabilities associated with plasma shaping. The most important 2D axisymmetric, *i.e.*, the toroidal mode number n=0, instability is known as a vertical instability, which becomes unstable once a plasma elongation is increased above a threshold. This instability is well understood to originate from a $J_{\phi,pl} \times B_{ext,pol}$ force on the plasma by an external equilibrium field due to a bad curvature associated with the plasma's shape. The field curvature can be evaluated by using a field decay index, $n_{\rm decay}$, defined as

$$n_{\rm decay}(R,Z) \equiv -\frac{R}{B_Z}\frac{\partial B_Z}{\partial R} = -\frac{R}{B_Z}\frac{\partial B_R}{\partial Z}. \qquad (18)$$

Theoretically, a vertically elongated plasma is well known possibly to be unstable when $n_{\rm decay} < 0$, and a radially elongated plasma may be unstable when $n_{\rm decay} > 3/2$ [21].

The relation between the plasma's shape and the field decay index can be seen in Fig. 3 for a plasma with $I_p = 0.5$ MA and $B_T = 2.5$ T, where theoretically stable and unstable regions are marked with filled colors. A comparison of the two plasmas with different values of beta (β_p) shows that the plasma with the higher β_p is less unstable and has a wider range of stable κ, which is consistent with theory. Note that a series of equilibria in this figure is obtained by specifying the plasma boundary (*i.e.*, as a *semi-free* boundary problem) in order to avoid the axisymmetric instability due to the bad curvature.

2. Generalized Stabilization for Axisymmetric Instabilities

Due to the axisymmetric instability, the direct solution of plasma equilibrium under a given external equilibrium field (*i.e.*, as an *ideally free* boundary problem) has a convergence problem. That is, a small deviation of the plasma from an equilibrium position is inevitable during a numerical iteration, so the plasma may drift and eventually diverge either radially (when $n_{decay} > 1.5$) or vertically (when $n_{decay} < 0.0$). In the literature, a conventional method to resolve the vertical instability of an elongated plasma is simply to insert a feedback loop [10] by adding artificial feedback coils, which are typically a pair of up-down symmetric coils, to produce a horizontal magnetic field. In this method, the feedback coil currents are adjusted to control the vertical position of the magnetic axis to a pre-selected target position according to the relation

$$I_{\rm feedback} = -{\rm sign}(Z_{\rm coil})\Big\{C_1(Z^{(n)}_{\rm mag} - Z_{\rm target}) + C_2(Z^{(n)}_{\rm mag} - Z^{(n-1)}_{\rm mag})\Big\}I_p, \qquad (19)$$

where $Z_{\rm target}$ is the desired vertical position of the magnetic axis and $Z_{\rm coil}$ is the vertical position of the control coil. A critical drawback of this method is that the desired vertical position of the magnetic axis has to be known prior to obtaining it as a solution from the equilibrium calculation. Also, the constants C_1 and C_2 are chosen by trial and error.

In the TES code, Eq. (19) is modified for a general treatment. Instead of controlling the vertical position in a feedback manner, we eliminate the source of the vertical instability by compensating for the B_R field at the center of the plasma currents in each step as follows:

$$I_{\rm feedback} = -g_z \left.\frac{B_{R,\rm vacuum}}{B^*_{R,\rm feedback}}\right|_{R_{\rm cur},Z_{\rm cur}}, \qquad (20)$$

where the minus sign indicates a compensation, g_z is an adjustable constant, and $B_{R,\rm vacuum}$ and $B^*_{R,\rm feedback}$ are the radial magnetic fields due to external equilibrium conductor currents (*i.e.*, vacuum field) and to unit currents of vertical stabilizing coils, respectively. Also, note that there is no I_P dependency in this method. If $g_z = 1.0$, the exact same B_R field is compensated for by using the feedback currents. In TES, practically, $2.0 \le g_z \le 2.5$ is used to ensure a general stabilization by using a up-down symmetric pair of coils, which is set to be radially centered and vertically just outside computational domain. For the evaluation of B_R, we use

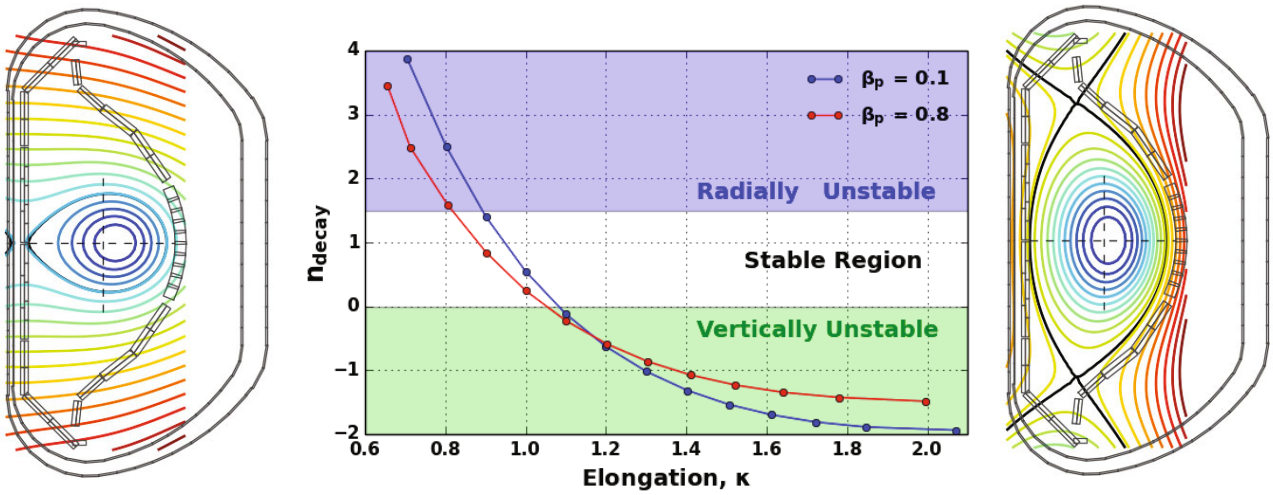

Fig. 3. (Color online) Decay index of external equilibrium fields ($n_{\rm decay}$) vs. plasma elongation (κ) for two different plasma betas (β_p). Theoretically stable and unstable regions in terms of $n_{\rm decay}$ are marked with filled colors. Additionally, a radially-elongated plasma with $\kappa = 0.7$ (left) and a vertically-elongated plasma with $\kappa = 2.0$ (right) are shown for $\beta_p = 0.8$.

the effective current center $(R_{\rm curr}, Z_{\rm curr})$ instead of the magnetic axis for a better description of an axisymmetric plasma's motion as follows:

$$R^2_{\rm cur} = \frac{1}{I_p}\int R^2 J_{\phi,pl}(R,Z)d\Omega_{pl}, \quad (21)$$
$$Z_{\rm cur} = \frac{1}{I_p}\int Z J_{\phi,pl}(R,Z)d\Omega_{pl}.$$

Note that a generalized method for the radial stabilization is not described here (due to lack of practical interest), but is also possible in a similar way.

3. Validation of Vertical Stability and Its Stabilization

For a validation of the generalized stabilization method described above, we first test the validity of the force-balance relation solved in TES by considering the natural axisymmetric instability. From Fig. 3, obviously the equilibrium with $\kappa = 1.2$ is expected to be vertically unstable ($n_{\rm decay} < 0$) while the equilibrium with $\kappa = 1.0$ is expected to be stable ($n_{\rm decay} > 0$) if the force-balance relation in TES is correct. Similarly, the equilibrium with $\kappa = 0.8$ is expected to be radially unstable ($n_{\rm decay} > 1.5$) while the equilibrium with $\kappa = 1.0$ is expected to be stable ($n_{\rm decay} < 1.5$). Remember that these equilibria were obtained by specifying the plasma boundary and, thus, produced the required external equilibrium fields (*i.e.*, as a *semi-free* boundary problem). To test the natural vertical stability without any additional stabilization, we re-performed the equilibrium analysis as an *ideally free* boundary problem, *i.e.*, by specifying the external equilibrium coil currents which were obtained from Fig. 3. As a seed for vertical or radial instability,

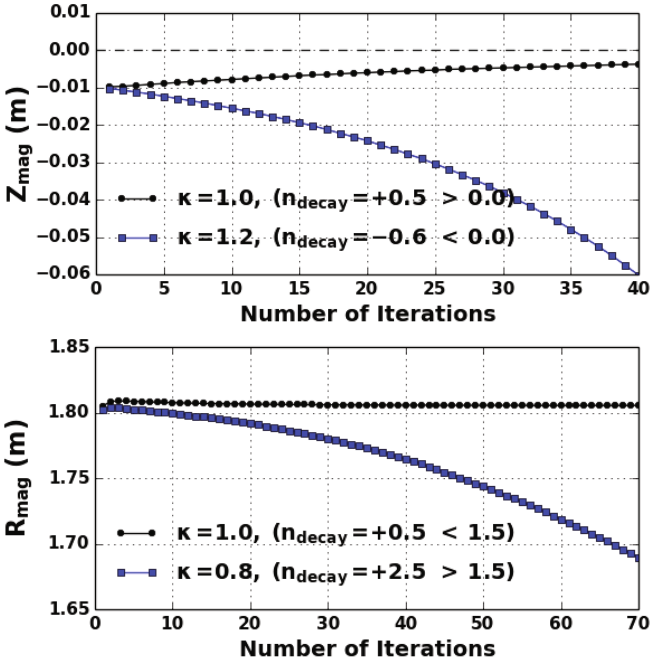

Fig. 4. (Color online) Comparisons of plasma displacement responses to the initial perturbations of $\Delta Z = -0.01$ m and $\Delta R = -0.01$ m for the stability test. Two equilibria with $\kappa = 1.0$ and $\kappa = 1.2$ are tested for the vertical stability (upper) and another two equilibria with $\kappa = 1.0$ and $\kappa = 0.8$ are tested for the radial stability (lower).

a small perturbation is added to the initial position of the plasma boundary, which is used in the 0-th Picard iteration.

The comparisons of vertical and radial displacement responses to small deviations of $\Delta Z = -0.01$ m and

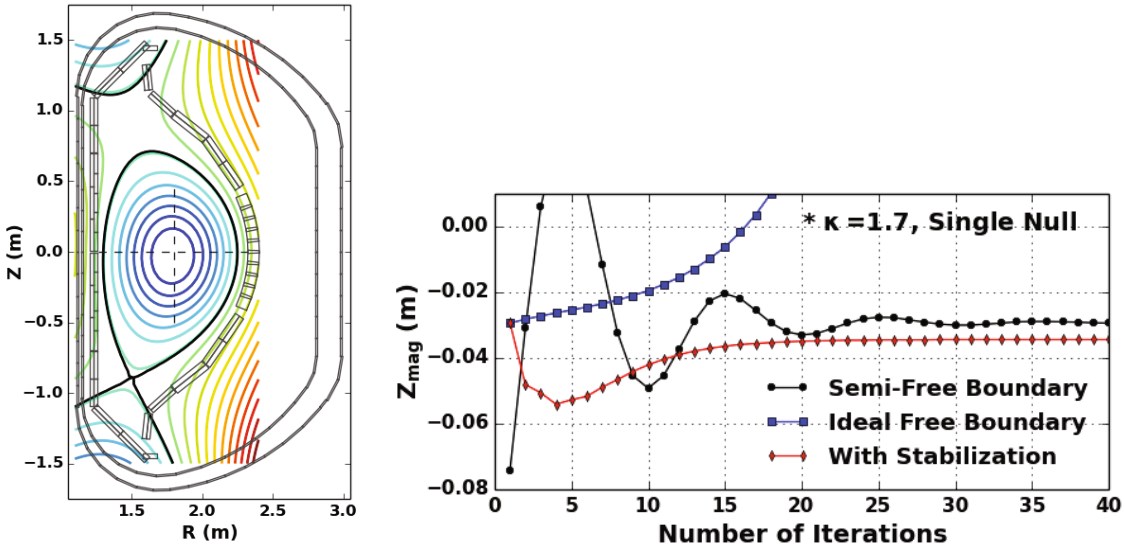

Fig. 5. (Color online) Vertical displacement responses to an initial perturbation of $\Delta Z = -0.03$ m are compared for the equilibrium shown on the left. The first one (black) is during TES iteration as a *semi-free* boundary problem, the second one (blue) as an *ideally-free* boundary problem, and the third one (red) with the generalized vertical stabilization.

$\Delta R = -0.01$ m are shown in Fig. 4. On the upper, the vertical stability is tested by an initial perturbation $\Delta Z = -0.01$ m for two equilibria; one with $\kappa = 1.0$ (black dotted line) and the other with $\kappa = 1.2$ (blue dotted line). Consistent with theoretical expectations, the initial perturbation of the former was naturally stabilized while that of the latter diverged exponentially. On the lower, the radial stability is tested by using an initial perturbation $\Delta R = -0.01$ m for two equilibria; one with $\kappa = 1.0$ (black dotted line) and the other with $\kappa = 0.8$ (blue dotted line). Similarly, the initial perturbation of the former was stable naturally while that of the latter diverged exponentially. This confirms that the force-balance relation used in TES is solved correctly, and the associated instability is consistent with the theory precisely.

For the validation of the generalized stabilization method, a further strongly shaped and up-down asymmetric plasma is considered as the worst case. The reference equilibrium is obtained in a single null (SN) configuration with $I_P = -0.5$ MA, $B_T = 2.5$ T, $\beta_P = 0.1$, and $\kappa = 1.7$ ($n_{\rm decay} = -1.8$) as shown in Fig. 5. The comparison of the vertical displacement responses with and without the generalized stabilization is shown on the right of Fig. 5. The evolution of a *semi-free* boundary solution (black line) shows that it converged to $Z_{\rm mag} = -0.03$ m (thus, it is a reference equilibrium position). In the case of the *ideally free* boundary solution (blue line) without any stabilization, it drifted upward and diverged, as expected. Then, when the generalized vertical stabilization (red line) was applied, the evolution was stabilized so that it evolved smoothly and closely converged to the reference position. Here, the final difference of vertical position from the reference position is about 0.5 cm, which demonstrates that the generalized method can effectively stabilize the natural vertical instability of elongated plasmas and automatically guide the plasma to an equilibrium position, which is consistent with the findings for a *semi-free* boundary solution.

V. EXTENSION TO AN ADVANCED EQUILIBRIUM ANALYSIS

Recently, new types of tokamak equilibria have been proposed and studied in various devices in order to resolve the issue of excessive heat and particle fluxes onto the plasma facing components in the International thermonuclear experimental reactor (ITER) and beyond. These are featured by a new divertor configuration, such as snow-flake [4] and (super) X divertors [5]. Particularly, the snow-flake equilibrium requires a second-order zero of the poloidal flux at the X-point. Therefore, dealing with it by a conventional free boundary equilibrium solver [8] is not straight-forward. Note that a typical X-point has a zero first-derivative of the poloidal flux (thus, a zero poloidal magnetic field), in contrast to the zero second-derivative of the poloidal flux in the snow-flake equilibrium. For this new equilibrium with a specified plasma boundary, the minimization constraint, Eq. (14), required for external equilibrium field currents is modified in TES as follows:

$$\min_{\Delta I_{\rm coil}} \Bigg[\sum_{j=1}^{N_{\rm bndry}} \left\{ \sum_{i=1}^{N_{\rm coil}} \Big(G(R_j,Z_j;R_i,Z_i)\cdot \Delta I_{{\rm coil},i} \Big) - \Delta\psi(R_j,Z_j) \right\}^2 + \sum_{j=1}^{N_{\rm Xpt}^{\rm SF}} \left\{ \sum_{i=1}^{N_{\rm coil}} \Big(\frac{\partial G_{B_R}(R_j,Z_j;R_i,Z_i)}{\partial Z}\cdot \Delta I_{{\rm coil},i} \Big) - \left.\frac{\partial B_R}{\partial Z}\right|_{(R_j,Z_j)} \right\}^2 + \sum_{j=1}^{N_{\rm Xpt}^{\rm SF}} \left\{ \sum_{i=1}^{N_{\rm coil}} \Big(\frac{\partial G_{B_Z}(R_j,Z_j;R_i,Z_i)}{\partial R}\cdot \Delta I_{{\rm coil},i} \Big) - \left.\frac{\partial B_Z}{\partial R}\right|_{(R_j,Z_j)} \right\}^2 + \gamma^2 \textstyle\sum_{i=1}^{N_{\rm coil}} \Big(\Delta I_{{\rm coil},i} \Big)^2 \Bigg], \tag{22}$$

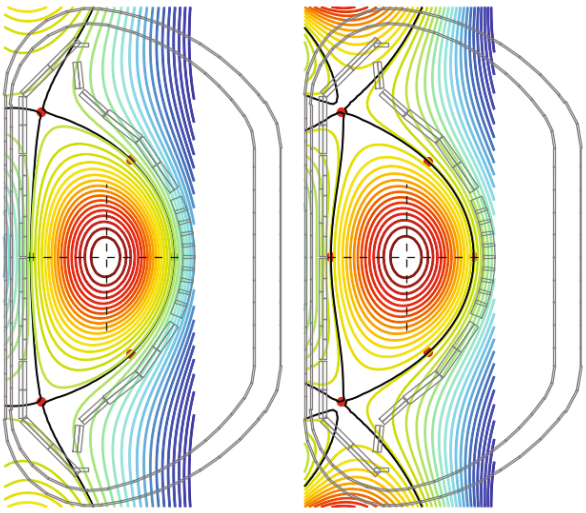

Fig. 6. (Color online) Comparison of two distinctive plasma equilibria. One is with a typical double-null divertor (left) and the other with a snow-flake divertor (right). The plasma boundary points specified in the calculation are marked with red circles.

where $\dfrac{\partial B_R}{\partial Z} = \dfrac{\partial}{\partial Z}\left(-\dfrac{1}{R}\dfrac{\partial \psi}{\partial Z}\right) = -\dfrac{1}{R}\dfrac{\partial^2 \psi}{\partial Z^2}$ and similarly $\dfrac{\partial B_Z}{\partial R} = +\dfrac{1}{R}\dfrac{\partial^2 \psi}{\partial R^2}$. With this, the snow-flake equilibrium that requires a second-order zero of $\psi(R,Z)$ can be directly obtained without any special treatment in TES.

Figure 6 shows a comparison of two equilibria obtained by TES with identical plasma equilibrium parameters, which are I_P =1.0 MA, B_T =2.5 T, κ =2.0, and β_P =0.2. One (on the left) is a typical double-null (DN) divertor and the other (on the right) is a snow-flake (SF) divertor configurations. The difference between the equilibria is easily seen from the magnetic distributions around the field null points. In the SF configuration, clearly, three concave and another three convex distributions are seen to be formed alternately, centred at the up-down symmetric field's null points; *i.e.*, a second-order zero of the poloidal magnetic flux is formed.

Table 1. External coil currents (kA) required to form the equilibria shown in Fig. 6

	Double-null (DN)	Snow-flake (SF)
PF1	−6.02	−1.04
PF2	9.64	−19.05
PF3	6.10	135.27
PF4	7.07	−67.32
PF5	8.33	18.60
PF6	−1.03	−5.30
PF7	−7.26	−4.03

Table 1 shows the external equilibrium coil currents required to form the target equilibria shown in Fig. 6. Worthy of note is that in the case of the SF equilibrium, some coil currents must have extremely large values while in the case of the DN equilibrium, all coil currents are well balanced. This indicates that forming the SF equilibria onto the KSTAR by using the current coil system is not practical. Therefore, a new coil system specially designed for the SF divertor is needed. In fact, this finding is consistent with a recently highlighted issue in a study on advanced divertor configurations [8]. In addition, worthy of note is that the SF equilibrium here is found self-consistently by considering full force-balance relations in a toroidal system while in the Ref. [8], it is found by using a simplified wire plasma model.

VI. CONCLUSIONS

A free-boundary tokamak equilibrium solver, developed for advanced study of tokamak equilibra, was described with various validation results. The developed solver, named as TES, is characterized by two distinctive features. First, a generalized stabilization method for the intrinsic axisymmetric instabilities was applied, which is encountered after all in equilibrium calculation under a free boundary condition. In this method, the source of axisymmetric instabilities is directly removed

or minimized, instead of feedback controlling the plasma position to a target location. Thus, it ensures in general that the TES code produces a solution stably even under highly (axisymmetrically) unstable conditions.

The other important feature is an extension to deal with a new divertor geometry such as snow-flake or X divertors. To deal with the innovative divertor concept, particularly the snow-flake divertor, the equilibrium solver needs to be able to control the location of the second-order zero of the poloidal magnetic field. By implementing this functionality into the TES code, we demonstrated that the snow-flake type of advanced tokamak equilibrium can be analyzed in consideration of the full toroidal force balance relations, instead of using a simplified wire plasma model.

For the validation of the TES code, the uniqueness of a solution was confirmed by the independence of the variations of the computational domain and grids. The mathematical correctness and accuracy of the equilibrium profiles were checked by using a direct comparison with the generalized Solov'ev analytic equilibrium. Additionally, the governing force balance relation was tested by examining the intrinsice axisymmetric instabilities.

As a valuable application, a snow-flake equilibrium was analyzed by taking into account the KSTAR equilibrium coil system. Because the KSTAR has a limited set of equilibrium control coils, checking whether the innovative divertor equilibria can be realized in the current system is important. The analysis results suggest that forming a snow-flake equilibrium in the current KSTAR device is not possible so additional control coils need to be considered for the study of advanced divertors in future.

ACKNOWLEDGMENTS

This work was supported by the Korean Ministry of Science, ICT and Future Planning under the KSTAR project and was partly supported by the JSPS-NRF-NSFC A3 Foresight Program (NRF No. 2012K2A2A6000443)

REFERENCES

[1] Tatsuoki Takeda and Shinji Tokuda, J. Comp. Phys. **93**, 1 (1991).
[2] V. D. Shafranov, ZhETF **33**, 710 (1957); Sov. Phys. JETP **8**, 494 (1958).
[3] H. Grad and H. Rubin, *Proceedings of 2nd International Conference on the Peaceful Uses of Atomics Energy 31*, (United Nations, Geneva, 1958), p. 190.
[4] D. D. Ryutov, Phys. Plasmas **14**, 064502 (2007).
[5] M. Kotschenreuther, P. M. Valanju, S. M. Mahajan and J. C. Wiley, Phys. Plasmas **14**, 072502 (2007).
[6] F. Piras *et al.*, Plasma Phys. Control. Fusion **51**, 055009 (2009).
[7] V. A. Soukhanovskii1 *et al.*, Nucl. Fusion **51**, 012001 (2011).
[8] K. Lackner and H. Zohm, Fusion Sci. Tech. **63**, 43 (2013).
[9] G. Lee *et al.*, Nucl. Fusion **40**, 575 (2000).
[10] J. L. Johnson *et al.*, J. Comp. Phys. **32**, 212 (1979).
[11] S. C. Jardin, N. Pomphrey and J. Delucia, J. Comp. Phys. **66**, 481 (1986).
[12] F. Hofmann, Comput. Phys. Commun. **48**, 207 (1988).
[13] R. Albanese and F. Villone, Nucl. Fusion **38**, 012001 (1998).
[14] H. P. William, A. T. Saul, T. V. William and P. F. Brian, *Numerical Recipes, 3rd Edition: The Art of Scientific Computing* (Cambridge University Press, New York, 2007).
[15] O. Buneman, Stanford University Institute for Plasma Research Rept. SUIPR-294 (1968).
[16] E. Kreyszig, *Advanced Engineering Mathematics*, 8^{th} Edition, (John Wiley & Sons, Hoboken, 1998).
[17] K. Miyamoto, *Plasma Physics for Nuclear Fusion*, revised Edition (The MIT Press, Cambridge, 1989).
[18] L. L. LoDestro and L. D. Pearlstein, Phys. Plasmas **1**, 90 (1994).
[19] A. N. Tikhonov and V. Y. Arsenin, *Solutions of Ill-posed Problems* (Winston and Sons,Washington, 1977).
[20] S. B. Zheng, A. J. Wootton and Emilia R. Solano, Phys. Plasmas **3**, 1176 (1996).
[21] A. Fukuyama, S. Seki, H. Momota and R. Itatani, Jpn. J. Appl. Phys **14**, 871 (1975).